





Classical Shadows with Improved Median-of-Means Estimation

Winston Fu ^{1,2} Dax Enshan Koh ^{1,2,3} Siong Thye Goh ^{1,2,4} and Jian Feng Kong ^{1,2}

¹Quantum Innovation Centre (Q.InC), Agency for Science, Technology and Research (A*STAR),
2 Fusionopolis Way, Innovis #08-03, Singapore 138634, Republic of Singapore

²Institute of High Performance Computing (IHPC), Agency for Science, Technology and Research (A*STAR),
1 Fusionopolis Way, #16-16 Connexis, Singapore 138632, Republic of Singapore

³Science, Mathematics and Technology Cluster, Singapore University of Technology and Design,
8 Somapah Road, Singapore 487372, Republic of Singapore

⁴Singapore Management University, 81 Victoria St, Singapore 188065, Republic of Singapore

The classical shadows protocol, introduced by Huang et al. [Nat. Phys. 16, 1050 (2020)], makes use of the median-of-means (MoM) estimator to efficiently estimate the expectation values of M observables with failure probability δ using only $\mathcal{O}(\log(M/\delta))$ measurements. In their analysis, Huang et al. used loose constants in their asymptotic performance bounds for simplicity. However, the specific values of these constants can significantly affect the number of shots used in practical implementations. To address this, we studied a modified MoM estimator proposed by Minsker [PMLR 195, 5925 (2023)] that uses optimal constants and involves a U-statistic over the data set. For efficient estimation, we implemented two types of incomplete U-statistics estimators, the first based on random sampling and the second based on cyclically permuted sampling. We compared the performance of the original and modified estimators when used with the classical shadows protocol with single-qubit Clifford unitaries (Pauli measurements) for an Ising spin chain, and global Clifford unitaries (Clifford measurements) for the Greenberger–Horne–Zeilinger (GHZ) state. While the original estimator outperformed the modified estimators for Pauli measurements, the modified estimators showed improved performance over the original estimator for Clifford measurements. Our findings highlight the importance of tailoring estimators to specific measurement settings to optimize the performance of the classical shadows protocol in practical applications.

I. INTRODUCTION

Classical shadows is a protocol recently proposed by Huang, Kueng, and Preskill [1] that builds on ideas from Aaronson’s shadow tomography [2] and quantum state tomography [3, 4] to efficiently estimate properties of an unknown quantum state ρ , without requiring a complete description of ρ to be learned. The protocol tackles the fundamental scaling problem of quantum systems, where learning a full description of the quantum system requires a number of measurements that scales exponentially with the number of qubits [5, 6]. By instead constructing an approximate classical description of the system, the expectation values of M observables can be predicted using only $\mathcal{O}(\log M)$ measurements, independent of system size. Since its introduction, the protocol and its variants [7–43] have found applications across diverse domains, including chemistry [44–48], machine learning [49–51], error mitigation [52, 53], entanglement characterization [54–56], and variational quantum algorithms [57–60], among others [61–66]. Moreover, noise-robust adaptations of the protocol have been introduced, allowing it to sustain efficient performance under realistic, noisy conditions [67–75].

To estimate expectation values of observables using classical shadows, the median-of-means (MoM) estimator [76, 77] is commonly employed, offering favorable scaling of sample complexity with respect to the failure probability of the protocol. In the original construction, Huang et al. chose conservative numerical constants for estimator bounds, which, although not affecting theoretical analyses, play a critical role in practical implementations

[78–81]. Specifically, these constants directly affect the number of measurements required to achieve a desired level of accuracy in the estimation process. While theoretical analyses typically focus on large sample sizes where constants become negligible, they become critical in practical scenarios with limited measurements or resource constraints. Tighter constants in the MoM estimator allow for more precise estimates with fewer measurements, reducing overhead.

Recently, Minsker [82, 83] presented optimal constants for the MoM estimator, and also proposed a modified version of the estimator with even tighter constants. In this study, we apply Minsker’s results to classical shadows. Using ideas from incomplete U-statistics [84], we introduce practical implementations of Minsker’s estimator which would otherwise be impossible to run for large datasets. Through numerical simulations, we benchmarked the performance of the original and modified estimators using an Ising spin chain and the Greenberger–Horne–Zeilinger (GHZ) state [85] to measure their performance, using the single-qubit Clifford unitary ensemble and global Clifford unitary ensemble respectively. We found that while the original MoM estimator performed better in the former case, the modified version showed improvements in the latter case.

The rest of our manuscript is structured as follows. In section II A, we review the basics of the classical shadows protocol. In section II B, we present the original MoM estimator used in the protocol, followed by Minsker’s modified estimator in section II C. Next, in section II D, we present two practical implementations of Minsker’s estimator using incomplete U-statistics in the context of

classical shadows. We then benchmark the estimators for the Ising spin chain in [section II E](#) and GHZ state in [section II F](#). Finally, in [section III](#), we provide a discussion of the results.

II. RESULTS

A. Classical Shadows

The purpose of the classical shadows protocol is to efficiently predict functions of a density matrix ρ . Of particular importance are linear functions, such as expectation values $\{o_i\}$ of a set of M observables $\{O_i\}$, which can be expressed as:

$$o_i(\rho) = \text{tr}(O_i\rho) \quad 1 \leq i \leq M. \quad (1)$$

The protocol works by applying a transformation $\rho \mapsto U\rho U^\dagger$, where U is randomly selected from an ensemble of unitaries. We consider two commonly used ensembles: random global Clifford unitaries, and tensor products of random single-qubit Clifford unitaries. After the transformation, we perform a computational-basis measurement to obtain $|\hat{b}\rangle \in \{0, 1\}^r$, where r is the number of qubits. Using this, we define the shadow channel \mathcal{M} , defined as

$$\mathcal{M}(\rho) = \mathbb{E}[U^\dagger|\hat{b}\rangle\langle\hat{b}|U]. \quad (2)$$

We typically choose ensembles for which the object $U^\dagger|\hat{b}\rangle\langle\hat{b}|U$ can be efficiently stored classically. Assuming that the inverse map \mathcal{M}^{-1} exists, it can be shown that the classical snapshot $\hat{\rho} = \mathcal{M}^{-1}(U^\dagger|\hat{b}\rangle\langle\hat{b}|U)$ is an unbiased estimator of ρ , i.e.,

$$\rho = \mathbb{E}[\hat{\rho}] = \mathbb{E}[\mathcal{M}^{-1}(U^\dagger|\hat{b}\rangle\langle\hat{b}|U)]. \quad (3)$$

While the inverse map \mathcal{M}^{-1} is not necessarily a valid quantum channel, it can still be applied during classical post-processing. Repeatedly sampling U from the ensemble of unitaries N times results in a classical shadow S of length N :

$$S(\rho; N) = \{\hat{\rho}_1, \dots, \hat{\rho}_N\}. \quad (4)$$

B. Median-of-Means Estimator

Given M observables O_i , which return $o_i = \text{tr}(O_i\rho)$ when acting on the system ρ , we can construct an unbiased estimator \hat{o}_i of o_i using the set of classical shadows $S(\rho; N)$:

$$\hat{o}_i(N, 1) = \frac{1}{N} \sum_{j=1}^N \text{tr}(O_i\hat{\rho}_j). \quad (5)$$

From Chebyshev's inequality,

$$P(|\hat{o}_i(N, 1) - \text{tr}(O_i\rho)| \geq \varepsilon) \leq \frac{\text{Var}[\hat{o}_i]}{\varepsilon^2} \quad (6)$$

$$= \frac{\text{Var}[\text{tr}(O_i\hat{\rho}_1)]}{N\varepsilon^2} \quad (7)$$

$$\equiv \frac{\delta}{M}. \quad (8)$$

This means that to achieve a failure probability below δ , the number of samples required scales as $N \sim 1/\delta$. To circumvent this $1/\delta$ dependence, the MoM estimator is often used:

$$\hat{o}_i(N, k) = \text{median} \left\{ \hat{o}_i^{(1)} \left(\left\lfloor \frac{N}{k} \right\rfloor, 1 \right), \dots, \hat{o}_i^{(k)} \left(\left\lfloor \frac{N}{k} \right\rfloor, 1 \right) \right\}. \quad (9)$$

This involves splitting the N snapshots into groups of size $\lfloor N/k \rfloor$, and finding the mean of each group. Then, we take the median of these groups. This procedure is shown in [Algorithm 1](#).

Algorithm 1 Median-of-means estimator for a list of data (MOM).

Input:

- x_1, \dots, x_N : Array of data.
- k : The number of disjoint subsets.

Output: Estimated result.

```

1: function MOM( $x_1, \dots, x_N, k$ )
2:    $A \leftarrow \{\}$ 
3:   for  $i \leftarrow 0, \lfloor \frac{N}{k} \rfloor - 1$  do
4:      $A \leftarrow A \cup \{\frac{1}{k} \sum_{p=i k+1}^{k(i+1)} x_p\}$ 
5:   end for
6:   return median( $A$ )
7: end function

```

Let $\hat{\mu}_{\text{MoM}}$ be an MoM estimator of N random variables X_i , so

$$\hat{\mu}_{\text{MoM}} = \text{median}(\bar{X}_1, \dots, \bar{X}_k), \quad (10)$$

where \bar{X}_i denotes the mean of the group with size $\lfloor N/k \rfloor$. The estimator $\hat{\mu}_{\text{MoM}}$ obeys the inequality

$$P\left(|\hat{\mu}_{\text{MoM}} - \mu| \geq C\sigma\sqrt{\frac{t}{N}}\right) \leq 2e^{-t}, \quad (11)$$

where C can be taken to be $8e^2$ (see [Appendix A](#)). Using $N = 34\sigma^2k/\varepsilon^2$, $t = k/2$, Huang et al. [[1](#)] obtain the bound

$$P(|\hat{\mu}_{\text{MoM}} - \mu| \geq \varepsilon) \leq 2e^{-k/2}. \quad (12)$$

However, Minsker [[83](#), [86](#)] showed that a tighter bound is possible.

Theorem 1 (Theorem 2.1 of Minsker [83].)

$$P\left(|\hat{\mu}_{\text{MoM}} - \mu| \geq \sigma \sqrt{\frac{t}{N}}\right) \leq 2 \exp\left(-\frac{t}{\pi}(1 + o(1))\right), \quad (13)$$

where $o(1)$ is a function that goes to 0 as $k, N/k \rightarrow \infty$, uniformly over $t \in [l_{k,N}, u_{k,N}]$ for any sequences $l_{k,N} \gg kg^2(N/k)$ and $u_{k,N} \ll k$, where g satisfies the following inequality:

$$g(m) \leq C \mathbb{E} \left| \frac{X_1 - \mu}{\sigma} \right|^q m^{-(q-2)/2} \quad (14)$$

whenever $\mathbb{E}|X_1 - \mu|^q < \infty$ for some $q \in (2, 3]$.

This corresponds to $C = \sqrt{\pi} + o(1)$ in Equation 11. In the context of quantum measurements, the condition $\mathbb{E}|X_1 - \mu|^q < \infty$ is trivially satisfied. Next, if $\sqrt{k}g(N/k) \rightarrow 0$ as $k, N \rightarrow \infty$, then the range of t becomes $1 \leq t \ll k$. For classical shadows, we can choose k such that $N \gg k$ and $o(1) \ll 1$. Hence, we will ignore this factor in our subsequent analysis.

Given M quantities we want to estimate, we construct the estimators $\hat{\mu}_1, \dots, \hat{\mu}_M$. We want to find a value for t such that:

$$P(|\hat{\mu}_i - \mu_i| \geq \varepsilon \forall i) \leq \delta. \quad (15)$$

Starting from Theorem 1, we make the substitution $t \mapsto \pi t$, $\varepsilon = \sigma \sqrt{\pi t/N}$:

$$P(|\hat{\mu}_i - \mu_i| \geq \varepsilon) \leq 2e^{-t} = \frac{\delta}{M}. \quad (16)$$

From the union bound,

$$P\left(\bigcup_{i=1}^M |\hat{\mu}_i - \mu_i| \geq \varepsilon\right) \leq \sum_{i=1}^M P(|\hat{\mu}_i - \mu_i| \geq \varepsilon) \quad (17)$$

$$\leq \sum_{i=1}^M \frac{\delta}{M} \quad (18)$$

$$= \delta. \quad (19)$$

Therefore, $t = \log(2M/\delta)$. To satisfy the condition $t \ll k$, we will choose $t = k/\log(k)$.

C. Modified Median-of-Means for Classical Shadows

Algorithm 2 Median-of-means estimator with combinations (MOMCOMB).

Input:

- x_1, \dots, x_N : Array of data.
- k : Changes the number of initial disjoint subsets, where kl is the number of subsets.
- l : Size of sets of sample averages.

Output: Estimated result.

```

1: function MOMCOMB( $x_1, \dots, x_N, k, l$ )
2:    $A \leftarrow \{\}$ 
3:   for  $i \leftarrow 0, \lfloor \frac{N}{kl} \rfloor - 1$  do           ▷ Split data into disjoint
      subsets, like in MOM.
4:      $A \leftarrow A \cup \{\frac{1}{kl} \sum_{j=ikl+1}^{kl(i+1)} x_j\}$ 
5:   end for

6:    $B \leftarrow$  all possible subsets of size  $l$  of  $A$    ▷  $B$  contains
       $\binom{kl}{l}$  sets of size  $l$ .
7:    $C \leftarrow \{\}$ 
8:   for all  $J \in B$  do
9:      $C \leftarrow C \cup \{\frac{1}{l} \sum_{p=1}^l J_p\}$ 
10:  end for
11:  return median( $C$ )
12: end function

```

It was shown by Minsker [82] that a modified, permutation-invariant version of MOM can give even tighter bounds. Similar to before, we first split our set of N data points $\{X_1, \dots, X_N\}$ into disjoint subsets of size $n = kl$ and take the mean of each subset:

$$G_1 \cup \dots \cup G_n \subseteq [N], \quad Z_j = \bar{X}_j = \frac{1}{|G_j|} \sum_{i \in G_j} X_i, \quad (20)$$

where $[N] = \{1, \dots, N\}$. For some set of integers $J \subseteq [n]$ of cardinality $|J| = l$, define $\bar{Z}_J = \frac{1}{l} \sum_{j \in J} Z_j$. Then, to construct our estimator $\hat{\mu}_{\text{comb}}$, we take the median of all possible \bar{Z}_J :

$$\hat{\mu}_{\text{comb}} \equiv \text{median}(\bar{Z}_J, J \in \mathcal{A}_n^{(l)}), \quad (21)$$

$$\mathcal{A}_n^{(l)} = \{J \subset [n] : |J| = l\}. \quad (22)$$

This process is shown in Algorithm 2.

Making appropriate substitutions to Minsker's results, we get a bound corresponding to $C = \sqrt{2} + o(1)$ in Equation 11—a tighter constant compared to MOM.

Theorem 2 (Theorem 1 of Minsker [82].) Assume that $\mathbb{E}|X_1 - \mu|^{2+a} < \infty$ for some $a > 0$. Suppose that $l = o(m^a)$ and let $L(n, l)$ and $M(n, l)$ be any sequences such that $L(n, l) \gg \frac{n}{l} g^2(m)$ and $M(n, l) \ll \frac{n}{l^2}$. Then for all $L(n, l) \leq t \leq M(n, l)$,

$$P\left(|\hat{\mu}_{\text{MoM}} - \mu| \geq \sigma \sqrt{\frac{t}{N}}\right) \leq 3 \exp\left(-\frac{t}{2(1 + o(1))}\right), \quad (23)$$

where $m = \lfloor N/k \rfloor$, $o(1) \rightarrow 0$ as $l, k \rightarrow \infty$ uniformly over all $t \in [L(n, l), M(n, l)]$.

A full treatment can be found in Minsker's [82] work. Using the same analysis as Equation 15, we choose $t = \log(3M/\delta)$. Additionally, we will use the values $l = \log(N/k)$, $t = n/l^2 \log(l)$.

Importantly, the performance of the **MOMCOMB** estimator is bounded by that of the U-statistic:

$$U_{n,l}(\rho'_-) = \binom{n}{l}^{-1} \sum_{J \in \mathcal{A}_n^{(l)}} \left(\rho'_-(\sqrt{m}(\bar{Z}_J - \mu - \sqrt{t/N}) - \mathbb{E} \rho'_-) \geq -\sqrt{k} \mathbb{E} \rho'_- \right), \quad (24)$$

where $\rho(x) = |x|$, ρ'_- is the left derivative of ρ , and

$$\mathbb{E} \rho'_- \equiv \mathbb{E} \rho'_- \left(\sqrt{m}(\bar{Z}_J - \mu - \sqrt{t/N}) \right). \quad (25)$$

One downside of this approach is its computational complexity of $\mathcal{O}(k^l \log k)$, which can quickly become untenable. A practical implementation therefore requires sampling a subset $D \subseteq \mathcal{A}_n^{(l)}$ of m elements. In the proceeding sections, we will draw heavily on analysis by Lee [84] to present and benchmark two possible methods of sampling: randomly, and using cyclic permutations.

D. Incomplete Modified Median-of-Means

Algorithm 3 Median-of-means estimator with random sampling (MOMRAND).

Input:

- x_1, \dots, x_N : Array of data.
- k : Changes the number of initial disjoint subsets, where kl is the number of subsets.
- l : Size of sets of sample averages.
- m : Number of randomly sampled sets of sample averages.

Output: Estimated result.

```

1: function MOMRAND( $x_1, \dots, x_N, k, l, m$ )
2:    $A \leftarrow \{\}$ 
3:   for  $i \leftarrow 0, \lfloor \frac{N}{kl} \rfloor - 1$  do           ▷ Split data into disjoint
      subsets, like in MOM.
4:      $A \leftarrow A \cup \{ \frac{1}{kl} \sum_{p=ikl+1}^{kl(i+1)} x_p \}$ 
5:   end for

6:    $B \leftarrow \{\}$ 
7:   for  $i \leftarrow 0, m - 1$  do ▷ Randomly sample  $m$  subsets of
       $A$ .
8:      $B \leftarrow B \cup \{ J \subseteq A : |J| = l \}$  where  $J$  is a random
      subset of  $A$ .
9:   end for

10:   $C \leftarrow \{\}$ 
11:  for all  $J \in B$  do
12:     $C \leftarrow C \cup \{ \frac{1}{l} \sum_{p=1}^l J_p \}$ 
13:  end for
14:  return median( $C$ )
15: end function

```

An incomplete U-statistic $U_n^{(0)}$ involves considering a subset \mathcal{D} of size m out of the $\binom{n}{l}$ terms in **MOMCOMB**, where \mathcal{D} is commonly called the design of $U_n^{(0)}$. For a given m , we want to choose \mathcal{D} to minimise the variance of $U_n^{(0)}$ to maximise the efficiency of the estimator.

A simple and common way of choosing the design is to randomly sample from $\mathcal{A}_n^{(l)}$ either with or without replacement. For simplicity, we will consider the former. This approach is shown in Algorithm 3. It can be shown that [84]

$$\text{Var } U_n^{(0)} = \frac{\sigma_l^2}{m} + (1 - m^{-1}) \text{Var } U_n, \quad (26)$$

where for some U-statistic $U_n = \binom{n}{l}^{-1} \sum_{(n,l)} \psi(X_{i_1}, \dots, X_{i_l})$ and the sum is taken over all permutations (i_1, \dots, i_l) of $\{1, 2, \dots, l\}$,

$$\sigma_c^2 = \text{Var}[\psi_c(X_1, \dots, X_c)], \quad (27)$$

where

$$\psi_c(x_1, \dots, x_c) = \mathbb{E}[\psi(X_1, \dots, X_k) | X_1 = x_1, \dots, X_c = x_c]. \quad (28)$$

Let $m = Kn$ for some constant K . Comparing the variance with the complete estimator U_n , we find the asymptotic relative efficiency (ARE)

$$\text{ARE} = \lim_{n \rightarrow \infty} \frac{\text{Var } U_n}{\text{Var } U_n^{(0)}} = \frac{Kl^2\sigma_1^2}{l^2\sigma_1^2 + \sigma_l^2}. \quad (29)$$

We can choose \mathcal{D} in a manner that is theoretically more efficient than simple random sampling. One possible minimum variance design employs cyclic permutations of our data set. To our data set of n elements Z_j , we apply the cyclic permutations

$$\begin{pmatrix} 1 & 2 & \dots & n \\ d_\nu \oplus 1 & d_\nu \oplus 2 & \dots & d_\nu \oplus n \end{pmatrix} \quad (30)$$

for $\nu = 1, 2, \dots, l$. The symbol \oplus denotes addition (mod n), and d_ν 's are chosen such that $(d_\nu - d_{\nu'}) \pmod{n}$ are distinct for any pair (ν, ν') with $\nu \neq \nu'$. In other words, the chosen d_ν must form a modified Golomb ruler [87], which can be found in $\mathcal{O}(l^2)$ time. Furthermore, the values of d_ν can be precomputed and stored in a lookup table for reference during the execution of the estimator. Hence, this step has minimal impact on the performance of the algorithm.

After applying each cyclic permutation with offset d_ν , the elements are sequentially grouped into sets of size l , with their average taken to give \bar{Z}_J . Repeating the process K times with a new set of d_ν , where all pairs d_ν used have distinct differences, gives a total of $m = Kn$ values for \bar{Z}_J . This is summarized in Algorithm 4.

This estimator **MOMCYC** has variance

$$\text{Var } U_n^{(0)} = m^{-1}(l(lK - 1)\sigma_1^2 + \sigma_l^2) \quad (31)$$

and

$$\text{ARE} = \frac{Kl^2\sigma_1^2}{l(lK - 1)\sigma_1^2 + \sigma_l^2}, \quad (32)$$

which is more efficient than **MOMRAND** for the same m .

Algorithm 4 Median-of-means estimator with cyclic permutations (**MOMCYC**).

Input:

- x_1, \dots, x_N : Array of data.
- k : Changes the number of initial disjoint subsets, where kl is the number of subsets.
- l : Size of sets of sample averages.
- m : Number of rounds.

Output: Estimated result.

\Rightarrow **CYCPERM**(A, d): cyclically permutes all elements in A by offset d .

\Rightarrow **GOLRUL**(l, D): generates a Golomb ruler (mod n) of length l , while also accounting for the differences stored in D .

```

1: function MOMCYC( $x_1, \dots, x_N, k, l, m$ )
2:    $A \leftarrow \{\}$ 
3:   for  $i \leftarrow 0, \lfloor \frac{N}{kl} \rfloor - 1$  do           ▷ Split data into disjoint
      subsets, like in MOM.
4:      $A \leftarrow A \cup \{\frac{1}{kl} \sum_{p=ikl+1}^{kl(i+1)} x_p\}$ 
5:   end for

6:    $B \leftarrow \{\}$ 
7:    $D \leftarrow \{\}$ 
8:   for  $i \leftarrow 0, m$  do
9:      $C \leftarrow \text{GOLRUL}(l, D)$ 
10:     $D \leftarrow$  differences between any two elements in  $C$ .
11:    for all  $d \in C$  do
12:      CYCPERM( $A, d$ )
13:      for  $j \leftarrow 0, \lfloor \frac{N}{kl^2} \rfloor - 1$  do           ▷ Split
      data into disjoint subsets of length  $l$  and store the mean
      of each subset.
14:         $B \leftarrow B \cup \{\frac{1}{l} \sum_{p=j+1}^{j+l} A_p\}$ 
15:      end for
16:    end for
17:  end for
18:  return median( $B$ )
19: end function

```

E. Benchmarking with Ising Chain

We first used classical shadows with random single-qubit Cliffords (hereby referred to as ‘Pauli measurements’) to estimate the two-point correlator function $\langle \sigma_1^z \sigma_{i+1}^z \rangle$ of a transverse field Ising model (TFIM), with Hamiltonian

$$H = J \sum_i \sigma_i^Z \sigma_{i+1}^Z + h \sum_i \sigma_i^X. \quad (33)$$

We found the correlator for 50 qubits with between 1000 and 50 000 Pauli measurements, using tensor network techniques described in section IV.

Figure 1 shows the results of the simulations using 4 different kinds of estimators. Figure 2 shows the difference between the predicted and exact values, together with the ‘Mean bound’ (Equation 8), ‘Huang-Kueng-Preskill (HKP) bound’ (Equation 12), ‘Original bound’ (Theorem 1), and

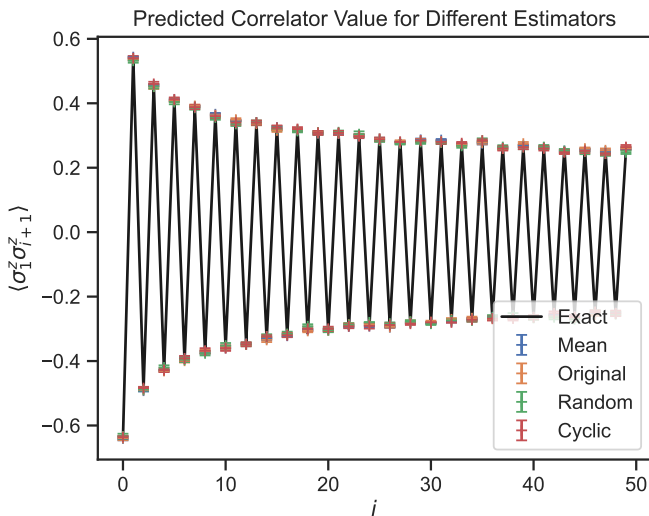


FIG. 1: Predicted and exact values for the 2-point correlator function over 50 qubits, using Pauli measurements.

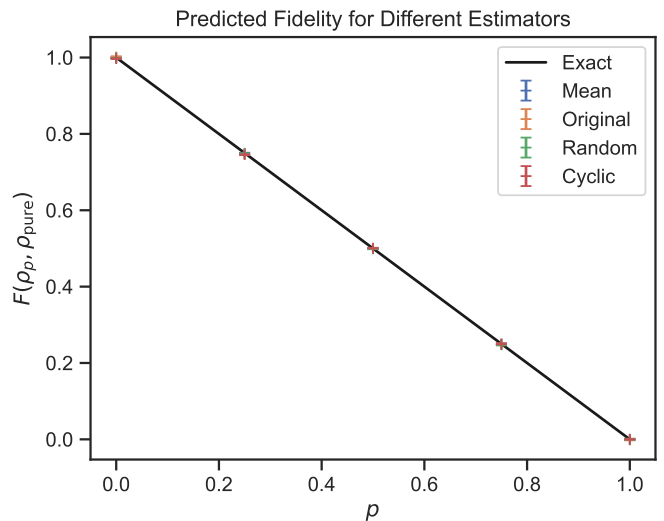


FIG. 3: Predicted and exact values of fidelity for different phase error probability p using Clifford measurements.

F. Benchmarking with Noisy GHZ State

Next, we examined the fidelity between a noisy GHZ state and a pure GHZ state. We define

$$|\text{GHZ}_r^\pm\rangle = \frac{1}{\sqrt{2}}(|0\rangle^{\otimes r} \pm |1\rangle^{\otimes r}) \quad (34)$$

and introduce a GHZ source which has a phase error with probability p

$$\rho_p = (1-p)|\text{GHZ}_r^+\rangle\langle\text{GHZ}_r^+| + p|\text{GHZ}_r^-\rangle\langle\text{GHZ}_r^-|. \quad (35)$$

Using Haar-random global Clifford unitaries (hereby referred to as ‘Clifford measurements’), we found the classical shadow of ρ_p and calculated the fidelity with the pure GHZ state $\rho_{\text{pure}} = |\text{GHZ}_r^+\rangle\langle\text{GHZ}_r^+|$,

$$F(\rho_p, \rho_{\text{pure}}) = \text{tr}(\rho_p \rho_{\text{pure}}). \quad (36)$$

Figure 3 shows the exact and predicted values of $F(\rho_p, \rho_{\text{pure}})$ for difference estimators and $r = 2$. Figure 4 shows the average error and variance.

Huang et al. [1] showed that the performance of the classical shadows protocol is independent of the number of qubits in the system. To verify this for the new estimators, we estimated the fidelity of the pure $p = 0$ GHZ state for $r = 5, 10, 15, 20$, and the average. This is shown in Figure 5. In this case, the 3.3σ value of MOM exceeds the bounds of the modified estimator (Theorem 2). Next, the shadow size N required to attain a fidelity of 0.98 was found, as shown in Figure 6, showing independence between accuracy and shadow size regardless of estimator.

Finally, we tested the estimators on quadratic functions of ρ . Instead of median of means, Huang et al. employ a median of U-statistics to estimate quadratic functions.

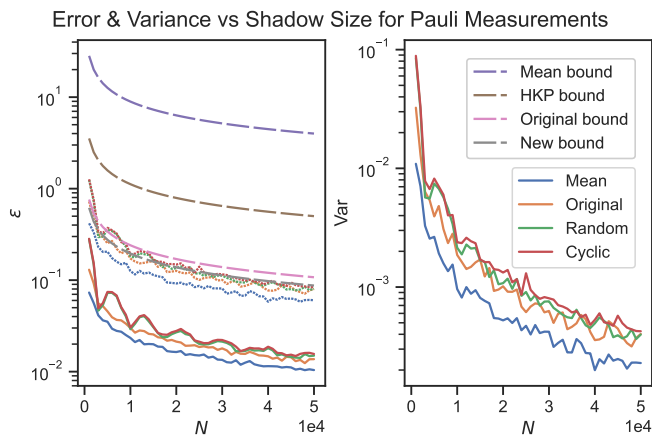


FIG. 2: (Left) Average error of each correlator over 10 runs against shadow size for the mean, MOM, MOMCOMB, MOMRAND, and MOMCYC. Short dotted lines of the corresponding color plot the 3.3σ boundary for each estimator. Long dashed lines show each of the bounds in Equation 8, Theorem 1, Theorem 2, and Equation 12. (Right) Variance for the same runs.

‘New bound’ (Theorem 2). The short dotted lines in the figure correspond to 3.3σ values, which have a 0.1% probability of occurring. This allows for direct comparison between numerical results and the theoretical bounds (long dashed lines) with failure probability $\delta = 0.1\%$.

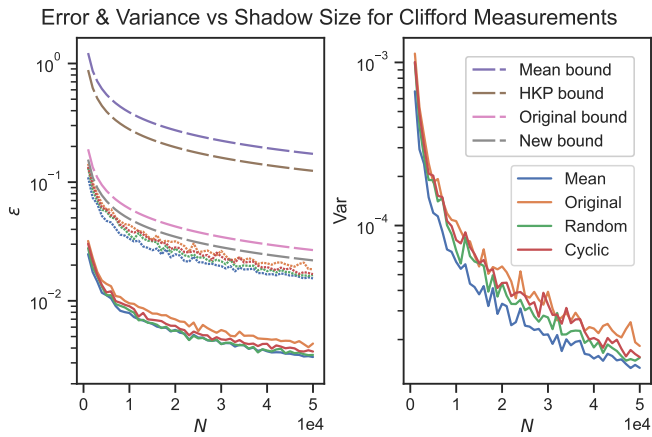


FIG. 4: (Left) Average error for the fidelity over 100 runs against shadow size for the mean, **MOM**, **MOMCOMB**, **MOMRAND**, and **MOMCYC** for the $n = 2$ -qubit noisy GHZ state. Short dotted lines of the corresponding color plot the 3.3σ boundary for each estimator. Long dashed lines show the bounds. (Right) Variance for the same runs.

The details of these modified estimators can be found in section IV.

Figure 7 shows the predicted purity for different values of p over 10 independent runs for $p = 0, 0.25, 0.5, 0.75, 1$, and Figure 8 shows the error and variances of each estimator.

III. DISCUSSION

Despite having the worst bound, taking the mean of the data had the lowest average error out of all the estimators. This agrees with prior experiments [78–80], as the distribution of the estimator $\hat{\rho}_i(N, 1)$ tends towards a normal distribution as $N \rightarrow \infty$ and gives a tighter bound than Theorem 2. Our results strengthen the case for the normality of $\hat{\rho}_i(N, 1)$ for the number of samples $N \geq 1000$ examined (Appendix B).

When estimating Pauli observables using Pauli measurements, **MOM** had the best performance out of the remaining estimators despite having worse bounds than **MOMRAND** and **MOMCYC**. **MOMRAND** had error that was in between **MOM** and **MOMCYC**. This result is further discussed in Appendix C. The 3.3σ error of **MOMRAND** and **MOMCYC** exceeded the tightened bounds by Minsker (Theorem 2), indicating that these estimators may not be suitable for use with Pauli measurements.

When using Clifford measurements to predict linear functions, the practical performance of the MoM estimators followed the tightened bounds closely, indicating the validity of the assumptions made. **MOM** now had higher error and variance than **MOMRAND** and **MOMCYC**. This shows that Minsker’s estimator offers an advantage over the traditional MoM protocol for Clifford measure-

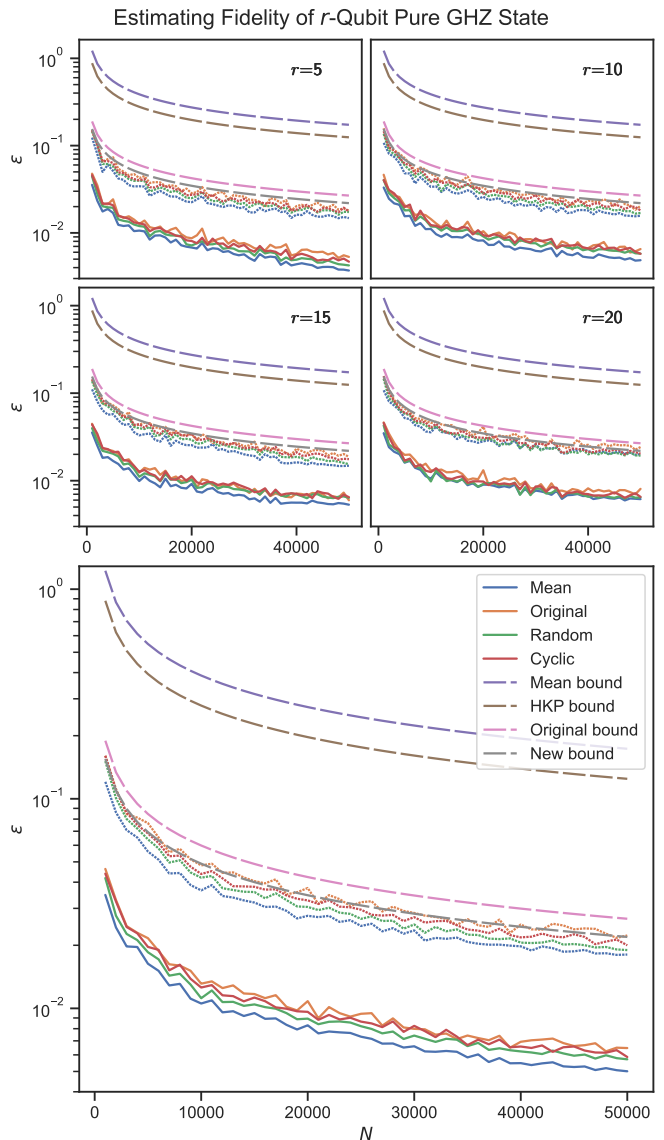


FIG. 5: (Top half): Error in fidelity with the r -Qubit pure GHZ state with $r = 5, 10, 15, 20$, over 10 independent runs. (Bottom half): Average error over all four values of n .

ments. In this case, the mean and **MOMRAND** performed similarly, while **MOMCYC** performed slightly worse. We have also demonstrated the tightness of Minsker’s bound (Theorem 2) in Figure 5, as the bound was exceeded by **MOM** but not **MOMRAND** and **MOMCYC**.

When predicting quadratic functions such as purity, the mean continued to perform the best. The **MOMRAND** and **MOMCYC** estimators had worse performance than **MOM**, in contrast to the improved performance for linear functions.

Despite the higher ARE of **MOMCYC** compared to **MOMRAND**, the latter showed better performance for Clifford measurements.

While the mean showed the best performance in all the

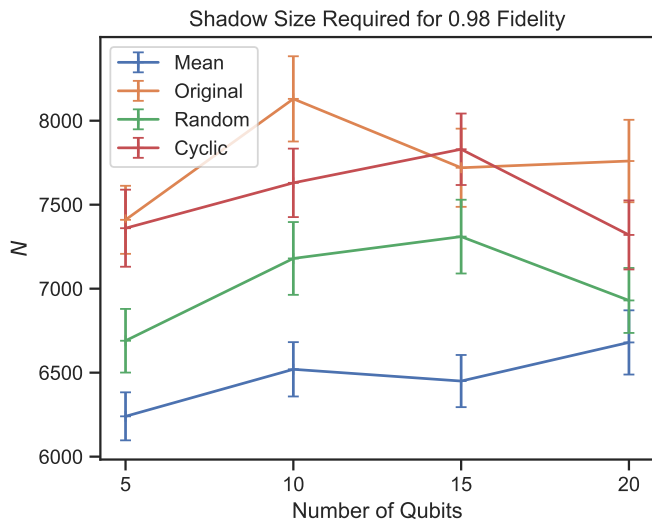


FIG. 6: Number of snapshots needed to achieve 0.98 fidelity ($\varepsilon < 0.02$) for increasing system size, using various estimators, Averaged over 10 independent runs.

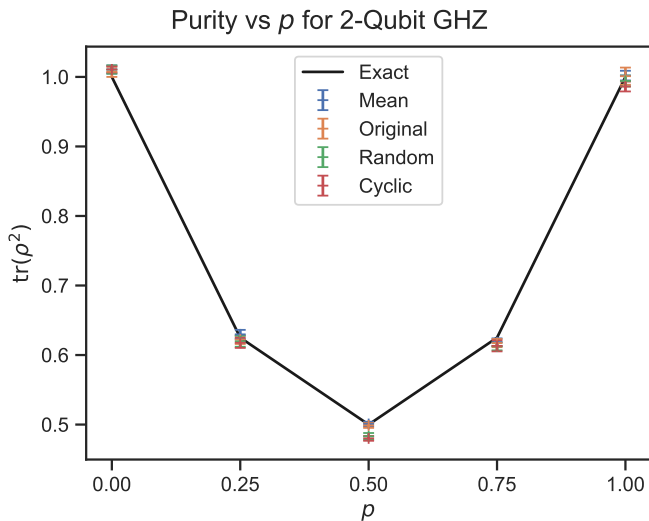


FIG. 7: Predicted purity for the 2-qubits GHZ state using mean, **MOM**, **MOMRAND**, and **MOMCYC**, for $p = 0, 0.25, 0.5, 0.75, 1$, and $N = 10\,000$ shadows.

simulations, **MOMRAND** had similar results when using Clifford measurements, with the added benefit that the MoM estimators are backed by performance bounds under weaker assumptions. Using the bound in [Theorem 2](#), the number of shots needed can be greatly reduced. As a simple illustration, the minimum number of shots required is summarized in [Table I](#) for an average error $M = 50$, $\varepsilon < 0.1$, $\delta = 0.001$. The loose bound used by Huang et al. requires several orders of magnitude more shots than the tighter bounds by Minsker.

As these changes happen purely in the classical post-processing step of the classical shadows protocol, our findings are immediately applicable to any experiment

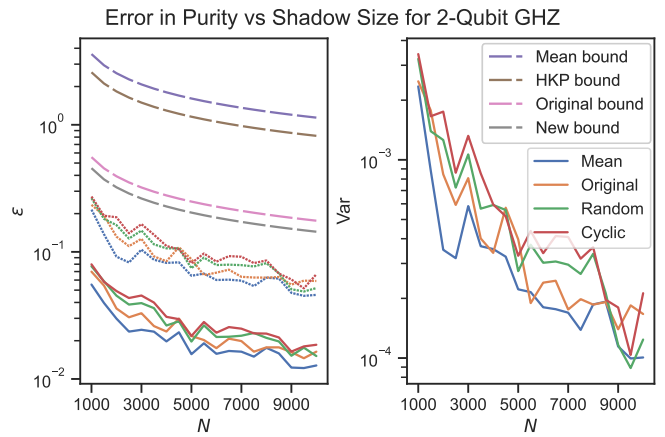


FIG. 8: Error and variance of predictions with varying shadow size N using different estimators and their associated bounds, averaged over $p = 0, 0.25, 0.5, 0.75, 1$ and 10 independent runs.

Bound	N
Mean	80×10^6
HKP	1.3×10^6
Original	58×10^3
New	38×10^3

TABLE I: Number of samples required to achieve an average error of $\varepsilon = 0.1$, using the different bounds.

that employs the protocol with no changes to the actual experimental design, as well as on existing datasets.

IV. METHODS

A. Pauli Measurements

The ground state of the Ising Hamiltonian was found using the infinite time-evolving block decimation (iTEBD) algorithm, in four steps of bond dimensions $\chi = 16, 32, 50, 100$ and time-steps $\tau = 0.1, 0.01, 0.001, 0.0001$ respectively. This was treated as the ground truth, and the matrix product state (MPS) tensors were used to find the classical shadow. The bit-string $\hat{b} = (\hat{b}_1, \dots, \hat{b}_r) \in \{0, 1\}^r$ was found using methods proposed by Ferris and Vidal [88]. 50 000 snapshots were taken for 10 independent experiments. Finally, the various estimators were used on the shadows with $M = 50$, $\delta = 0.001$. For **MOMRAND** and **MOMCYC**, the number of samples was chosen to be $m = 10kl$.

To generate shadows of size between 1000 and 50 000, the appropriate number of snapshots was randomly sampled from the full shadow. The single-qubit Clifford unitary U_j applied to each qubit was stored and used to

reconstruct each snapshot

$$\hat{\rho} = \bigotimes_{j=1}^r \left(3U_j^\dagger |\hat{b}_j\rangle \langle \hat{b}_j| U_j - \mathbb{1} \right). \quad (37)$$

B. Clifford Measurements

The GHZ state was simulated efficiently using the stabilizer formalism, implemented using the Qiskit library. Using the global Clifford ensemble, it can be shown that the snapshots have the form

$$\hat{\rho} = (2^r + 1)U^\dagger |\hat{b}\rangle \langle \hat{b}| U - \mathbb{1}. \quad (38)$$

When estimating fidelity we can use this form to show:

$$F(\rho_0, \hat{\rho}) = (2^r + 1) |\langle \hat{b}| U | \text{GHZ}^+(r) \rangle|^2 - 1. \quad (39)$$

The shadows of the 2-qubit GHZ state were found for $p = 0, 0.25, 0.5, 0.75, 1$, for 100 independent runs and shadow size $N = 50\,000$. To estimate the fidelity for $1000 \leq N \leq 50\,000$, the appropriate number of snapshots was sampled randomly from the full shadow.

Next, 10 shadows of the $r = 5, 10, 15, 20$ GHZ states were found for $p = 0$. For each shadow, 10 fidelity estimates were obtained for each value of $1000 \leq N \leq 50\,000$, sampled randomly, using each of the estimators, to obtain 100 runs. To find the minimum number of snapshots for 0.98 fidelity, a rolling average over 5 values of N was used to smooth out the data, then the minimum N was found for each run, before taking the average.

To estimate purity,

$$\text{tr}(U_{\text{swap}} \hat{\rho}_1 \otimes \hat{\rho}_2) = (2^r + 1)^2 |\langle \hat{b}_1 | U_1 U_2^\dagger | \hat{b}_2 \rangle|^2 - 2(2^r + 1) + 2^r, \quad (40)$$

where U_{swap} is the SWAP operator. Instead of taking the median-of-means of disjoint subsets, we instead used each subset to find the U-statistic:

$$\begin{aligned} & \hat{o}_i^{(q)} \left(\left\lfloor \frac{N}{k} \right\rfloor, 1 \right) \\ &= \frac{1}{\left\lfloor \frac{N}{k} \right\rfloor \left(\left\lfloor \frac{N}{k} \right\rfloor - 1 \right)} \sum_{\substack{u \neq v \\ u, v \in \{N(1-\frac{1}{q})+1, \dots, N\}}} \text{tr}(O_i \hat{\rho}_u \otimes \hat{\rho}_v) \end{aligned} \quad (41)$$

for $1 \leq q \leq k$. Then, we took the median of this set of U-statistics:

$$\hat{o}_i(N, k) = \text{median} \left\{ \hat{o}_i^{(1)} \left(\left\lfloor \frac{N}{k} \right\rfloor, 1 \right), \dots, \hat{o}_i^{(k)} \left(\left\lfloor \frac{N}{k} \right\rfloor, 1 \right) \right\}. \quad (42)$$

We define the ‘mean’ estimator to be the mean of the set of $\hat{o}_i^{(p)}(N, 1)$ from which the median is found for **MOM**.

To extend this estimator to **MOMRAND** and **MOMCYC**, we treated this U-statistic as the mean in the first step of the algorithm (line 4 of Algorithms 3 and 4), then grouped them to form \bar{Z}_J . This was used to estimate the purity $\text{tr}(\rho^2) = \text{tr}(U_{\text{swap}} \rho \otimes \rho)$ of the $n = 2$ noisy GHZ state for $p = 0, 0.25, 0.5, 0.75, 1$ from 10 shadows for $1000 \leq N \leq 10000$.

ACKNOWLEDGEMENTS

This research is supported by the National Research Foundation, Singapore, and the Agency for Science, Technology and Research (A*STAR), Singapore, under its Quantum Engineering Programme (NRF2021-QEP2-02-P03); A*STAR C230917003; and A*STAR under the Central Research Fund (CRF) Award for Use-Inspired Basic Research (UIBR) and the Quantum Innovation Centre (Q.InC) Strategic Research and Translational Thrust.

-
- [1] H.-Y. Huang, R. Kueng, and J. Preskill, Predicting many properties of a quantum system from very few measurements, *Nature Physics* **16**, 1050 (2020).
 - [2] S. Aaronson, Shadow tomography of quantum states, in *Proceedings of the 50th Annual ACM SIGACT Symposium on Theory of Computing*, STOC 2018 (Association for Computing Machinery, New York, NY, USA, 2018) p. 325–338.
 - [3] M. Guță, J. Kahn, R. Kueng, and J. A. Tropp, Fast state tomography with optimal error bounds, *Journal of Physics A: Mathematical and Theoretical* **53**, 204001 (2020).
 - [4] T. Sugiyama, P. S. Turner, and M. Murao, Precision-Guaranteed Quantum Tomography, *Physical Review Letters* **111**, 160406 (2013).
 - [5] J. Haah, A. Harrow, Z. Ji, X. Wu, and N. Yu, Sample-Optimal Tomography of Quantum States, *IEEE Transactions on Information Theory* **63**, 5628 (2017).
 - [6] R. O’Donnell and J. Wright, Efficient quantum tomography, in *Proceedings of the forty-eighth annual ACM symposium on Theory of Computing* (2016) pp. 899–912.
 - [7] J. M. Lukens, K. J. Law, and R. S. Bennink, A Bayesian analysis of classical shadows, *npj Quantum Information* **7**, 113 (2021).
 - [8] H.-Y. Huang, R. Kueng, and J. Preskill, Efficient Estimation of Pauli Observables by Derandomization, *Physical Review Letters* **127**, 030503 (2021).
 - [9] C. Hadfield, Adaptive Pauli shadows for energy estimation, *arXiv preprint 2105.12207* (2021).
 - [10] A. Zhao, N. C. Rubin, and A. Miyake, Fermionic partial tomography via classical shadows, *Physical Review Letters* **127**, 110504 (2021).
 - [11] C. Hadfield, S. Bravyi, R. Raymond, and A. Mezzacapo, Measurements of Quantum Hamiltonians with Locally-Biased Classical Shadows, *Communications in Mathemat-*

- ical Physics **391**, 951 (2022).
- [12] Y. Zhou and Z. Liu, A hybrid framework for estimating nonlinear functions of quantum states, *npj Quantum Information* **10**, 62 (2024).
- [13] A. A. Akhtar, H.-Y. Hu, and Y.-Z. You, Scalable and Flexible Classical Shadow Tomography with Tensor Networks, *Quantum* **7**, 1026 (2023).
- [14] H.-Y. Hu, S. Choi, and Y.-Z. You, Classical shadow tomography with locally scrambled quantum dynamics, *Physical Review Research* **5**, 023027 (2023).
- [15] S. Shivam, C. W. von Keyserlingk, and S. L. Sondhi, On classical and hybrid shadows of quantum states, *SciPost Phys.* **14**, 094 (2023).
- [16] A. A. Akhtar, H.-Y. Hu, and Y.-Z. You, Scalable and Flexible Classical Shadow Tomography with Tensor Networks, *Quantum* **7**, 1026 (2023).
- [17] K. Wan, W. J. Huggins, J. Lee, and R. Babbush, Matchgate shadows for fermionic quantum simulation, *Communications in Mathematical Physics* **404**, 629 (2023).
- [18] L. Innocenti, S. Lorenzo, I. Palmisano, F. Albarelli, A. Ferraro, M. Paternostro, and G. M. Palma, Shadow tomography on general measurement frames, *PRX Quantum* **4**, 040328 (2023).
- [19] M. Ippoliti, Y. Li, T. Rakovszky, and V. Khemani, Operator relaxation and the optimal depth of classical shadows, *Phys. Rev. Lett.* **130**, 230403 (2023).
- [20] J. Helsen and M. Walter, Thrifty shadow estimation: Reusing quantum circuits and bounding tails, *Phys. Rev. Lett.* **131**, 240602 (2023).
- [21] D. Grier, H. Pashayan, and L. Schaeffer, Principal eigenstate classical shadows, in *Proceedings of Thirty Seventh Conference on Learning Theory*, Proceedings of Machine Learning Research, Vol. 247, edited by S. Agrawal and A. Roth (PMLR, 2024) pp. 2122–2165.
- [22] F. Sauvage and M. Larocca, Classical shadows with symmetries, *arXiv preprint arXiv:2408.05279* (2024).
- [23] K. Bu, D. E. Koh, R. J. Garcia, and A. Jaffe, Classical shadows with Pauli-invariant unitary ensembles, *npj Quantum Information* **10**, 6 (2024).
- [24] D. Grier, H. Pashayan, and L. Schaeffer, Sample-optimal classical shadows for pure states, *Quantum* **8**, 1373 (2024).
- [25] M. West, A. A. Mele, M. Larocca, and M. Cerezo, Real classical shadows, *arXiv preprint arXiv:2410.23481* (2024).
- [26] M. Ippoliti, Classical shadows based on locally-entangled measurements, *Quantum* **8**, 1293 (2024).
- [27] R. King, D. Gosset, R. Kothari, and R. Babbush, Triply efficient shadow tomography, *arXiv preprint arXiv:2404.19211* (2024).
- [28] G. De Palma, T. Klein, and D. Pastorello, Classical shadows meet quantum optimal mass transport, *Journal of Mathematical Physics* **65**, 092201 (2024).
- [29] S. Becker, N. Datta, L. Lami, and C. Rouze, Classical shadow tomography for continuous variables quantum systems, *IEEE Transactions on Information Theory* **70**, 3427 (2024).
- [30] S. N. Hearth, M. O. Flynn, A. Chandran, and C. R. Laumann, Efficient local classical shadow tomography with number conservation, *Phys. Rev. Lett.* **133**, 060802 (2024).
- [31] Z. Cai, A. Chapman, H. Jnane, and B. Koczor, Biased estimator channels for classical shadows, *arXiv preprint arXiv:2402.09511* (2024).
- [32] D. T. S. Chen, Z. H. Saleem, and M. A. Perlin, Quantum circuit cutting for classical shadows, *ACM Transactions on Quantum Computing* **5**(2), 13 (2024).
- [33] V. Heyraud, H. Chomet, and J. Tilly, Unified framework for matchgate classical shadows, *arXiv preprint arXiv:2409.03836* (2024).
- [34] A. A. Akhtar, N. Anand, J. Marshall, and Y.-Z. You, Dual-unitary classical shadow tomography, *arXiv preprint arXiv:2404.01068* (2024).
- [35] Y. Wang, Quantum advantage via efficient post-processing on qudit shadow tomography, *arXiv preprint arXiv:2408.16244* (2024).
- [36] Y. Wu, C. Wang, J. Yao, H. Zhai, Y.-Z. You, and P. Zhang, Contractive unitary and classical shadow tomography, *arXiv preprint arXiv:2412.01850* (2024).
- [37] T.-G. Zhou and P. Zhang, Efficient Classical Shadow Tomography through Many-body Localization Dynamics, *Quantum* **8**, 1467 (2024).
- [38] R. Cioli, E. Ercolessi, M. Ippoliti, X. Turkishi, and L. Piroli, Approximate inverse measurement channel for shallow shadows, *arXiv preprint arXiv:2407.11813* (2024).
- [39] Q. Liu, Z. Li, X. Yuan, H. Zhu, and Y. Zhou, Auxiliary-free replica shadow estimation, *arXiv preprint arXiv:2407.20865* (2024).
- [40] C. Bertoni, J. Haferkamp, M. Hinsche, M. Ioannou, J. Eisert, and H. Pashayan, Shallow shadows: Expectation estimation using low-depth random Clifford circuits, *Phys. Rev. Lett.* **133**, 020602 (2024).
- [41] G.-L. R. Anselmetti, M. Degroote, N. Moll, R. Santagati, and M. Streif, Classical optimisation of reduced density matrix estimations with classical shadows using N-representability conditions under shot noise considerations, *arXiv preprint arXiv:2411.18430* (2024).
- [42] C. Mao, C. Yi, and H. Zhu, The magic in qudit shadow estimation based on the Clifford group, *arXiv preprint arXiv:2410.13572* (2024).
- [43] A. Caprotti, J. Morris, and B. Dakić, Optimizing quantum tomography via shadow inversion, *Phys. Rev. Res.* **6**, 033301 (2024).
- [44] Z.-J. Zhang, K. Nakaji, M. Choi, and A. Aspuru-Guzik, A composite measurement scheme for efficient quantum observable estimation, *arXiv preprint arXiv:2305.02439* (2023).
- [45] B. Huang, Y.-T. Chen, B. Gupt, M. Suchara, A. Tran, S. McArdle, and G. Galli, Evaluating a quantum-classical quantum Monte Carlo algorithm with matchgate shadows, *Phys. Rev. Res.* **6**, 043063 (2024).
- [46] I. Avdic and D. A. Mazziotti, Enhanced shadow tomography of molecular excited states via the enforcement of N-representability conditions by semidefinite programming, *Phys. Rev. A* **110**, 052407 (2024).
- [47] Y. Wang, I. Avdic, and D. A. Mazziotti, Shadow ansatz for the many-fermion wave function in scalable molecular simulations on quantum computing devices, *arXiv preprint arXiv:2408.11026* (2024).
- [48] I. Avdic and D. A. Mazziotti, Fewer measurements from shadow tomography with N-representability conditions, *Phys. Rev. Lett.* **132**, 220802 (2024).
- [49] H.-Y. Huang, R. Kueng, G. Torlai, V. V. Albert, and J. Preskill, Provably efficient machine learning for quantum many-body problems, *Science* **377**, eabk3333 (2022).
- [50] L. Lewis, H.-Y. Huang, V. T. Tran, S. Lehner, R. Kueng, and J. Preskill, Improved machine learning algorithm for predicting ground state properties, *Nature Communica-*

- tions **15**, 895 (2024).
- [51] S. Jerbi, C. Gyurik, S. C. Marshall, R. Molteni, and V. Dunjko, Shadows of quantum machine learning, *Nature Communications* **15**, 5676 (2024).
- [52] A. Zhao and A. Miyake, Group-theoretic error mitigation enabled by classical shadows and symmetries, *npj Quantum Information* **10**, 57 (2024).
- [53] A. Seif, Z.-P. Cian, S. Zhou, S. Chen, and L. Jiang, Shadow Distillation: Quantum Error Mitigation with Classical Shadows for Near-Term Quantum Processors, *PRX Quantum* **4**, 010303 (2023).
- [54] A. Elben, R. Kueng, H.-Y. R. Huang, R. van Bijnen, C. Kokail, M. Dalmonte, P. Calabrese, B. Kraus, J. Preskill, P. Zoller, and B. Vermersch, Mixed-state entanglement from local randomized measurements, *Phys. Rev. Lett.* **125**, 200501 (2020).
- [55] A. Neven, J. Carrasco, V. Vitale, C. Kokail, A. Elben, M. Dalmonte, P. Calabrese, P. Zoller, B. Vermersch, R. Kueng, *et al.*, Symmetry-resolved entanglement detection using partial transpose moments, *npj Quantum Information* **7**, 152 (2021).
- [56] A. Rath, C. Branciard, A. Minguzzi, and B. Vermersch, Quantum Fisher information from randomized measurements, *Phys. Rev. Lett.* **127**, 260501 (2021).
- [57] G. Boyd and B. Koczor, Training variational quantum circuits with CoVaR: Covariance root finding with classical shadows, *Phys. Rev. X* **12**, 041022 (2022).
- [58] S. H. Sack, R. A. Medina, A. A. Michailidis, R. Kueng, and M. Serbyn, Avoiding Barren Plateaus Using Classical Shadows, *PRX Quantum* **3**, 020365 (2022).
- [59] A. Basheer, Y. Feng, C. Ferrie, and S. Li, Alternating layered variational quantum circuits can be classically optimized efficiently using classical shadows, in *Proceedings of the AAAI Conference on Artificial Intelligence*, Vol. 37 (2023) pp. 6770–6778.
- [60] K. Nakaji, S. Endo, Y. Matsuzaki, and H. Hakoshima, Measurement optimization of variational quantum simulation by classical shadow and derandomization, *Quantum* **7**, 995 (2023).
- [61] R. J. Garcia, Y. Zhou, and A. Jaffe, Quantum scrambling with classical shadows, *Phys. Rev. Res.* **3**, 033155 (2021).
- [62] J. Helsen, M. Ioannou, J. Kitzinger, E. Onorati, A. Werner, J. Eisert, and I. Roth, Shadow estimation of gate-set properties from random sequences, *Nature Communications* **14**, 5039 (2023).
- [63] G. A. L. White, K. Modi, and C. D. Hill, Filtering crosstalk from bath non-Markovianity via spacetime classical shadows, *Phys. Rev. Lett.* **130**, 160401 (2023).
- [64] M. Ippoliti and V. Khemani, Learnability transitions in monitored quantum dynamics via eavesdropper’s classical shadows, *PRX Quantum* **5**, 020304 (2024).
- [65] E. A. Ruiz Guzman and D. Lacroix, Restoring symmetries in quantum computing using classical shadows, *The European Physical Journal A* **60**, 1 (2024).
- [66] J. Conrad, J. Eisert, and S. T. Flammia, Chasing shadows with Gottesman-Kitaev-Preskill codes, *arXiv preprint arXiv:2411.00235* (2024).
- [67] S. Chen, W. Yu, P. Zeng, and S. T. Flammia, Robust Shadow Estimation, *PRX Quantum* **2**, 030348 (2021).
- [68] D. E. Koh and S. Grewal, Classical Shadows With Noise, *Quantum* **6**, 776 (2022).
- [69] R. Brieger, M. Heinrich, I. Roth, and M. Kliesch, Stability of classical shadows under gate-dependent noise, *arXiv preprint arXiv:2310.19947* (2023).
- [70] H.-C. Nguyen, Shadow tomography with noisy readouts, *arXiv preprint arXiv:2310.17328* (2023).
- [71] B. Wu and D. E. Koh, Error-mitigated fermionic classical shadows on noisy quantum devices, *npj Quantum Information* **10**, 39 (2024).
- [72] P.-G. Rozon, N. Bao, and K. Agarwal, Optimal twirling depth for classical shadows in the presence of noise, *Physical Review Letters* **133**, 130803 (2024).
- [73] H. Jnane, J. Steinberg, Z. Cai, H. C. Nguyen, and B. Koczor, Quantum error mitigated classical shadows, *PRX Quantum* **5**, 010324 (2024).
- [74] R. Farias, R. D. Peddinti, I. Roth, and L. Aolita, Robust shallow shadows, *arXiv preprint arXiv:2405.06022* (2024).
- [75] E. Onorati, J. Kitzinger, J. Helsen, M. Ioannou, A. Werner, I. Roth, and J. Eisert, Noise-mitigated randomized measurements and self-calibrating shadow estimation, *arXiv preprint arXiv:2403.04751* (2024).
- [76] L. Devroye, M. Lerasle, G. Lugosi, and R. I. Oliveira, Sub-Gaussian mean estimators, *The Annals of Statistics* **44**, 2695 (2016).
- [77] G. Lugosi and S. Mendelson, Mean Estimation and Regression Under Heavy-Tailed Distributions: A Survey, *Foundations of Computational Mathematics* **19**, 1145 (2019).
- [78] G. Struchalin, Ya. A. Zagorovskii, E. Kovlakov, S. Straupe, and S. Kulik, Experimental Estimation of Quantum State Properties from Classical Shadows, *PRX Quantum* **2**, 010307 (2021).
- [79] T. Zhang, J. Sun, X.-X. Fang, X.-M. Zhang, X. Yuan, and H. Lu, Experimental Quantum State Measurement with Classical Shadows, *Physical Review Letters* **127**, 200501 (2021).
- [80] R. Levy, D. Luo, and B. K. Clark, Classical shadows for quantum process tomography on near-term quantum computers, *Physical Review Research* **6**, 013029 (2024).
- [81] A. Dutt, W. Kirby, R. Raymond, C. Hadfield, S. Sheldon, I. L. Chuang, and A. Mezzacapo, Practical Benchmarking of Randomized Measurement Methods for Quantum Chemistry Hamiltonians, *arXiv preprint arXiv:2312.07497* (2023).
- [82] S. Minsker, Efficient median of means estimator, in *Proceedings of Thirty Sixth Conference on Learning Theory*, Proceedings of Machine Learning Research, Vol. 195, edited by G. Neu and L. Rosasco (PMLR, 2023) pp. 5925–5933.
- [83] S. Minsker, U-statistics of growing order and sub-Gaussian mean estimators with sharp constants, *Mathematical Statistics and Learning* **7**, 1 (2023).
- [84] A. J. Lee, *U-Statistics: Theory and Practice* (Routledge, New York, 2019).
- [85] D. M. Greenberger, M. A. Horne, and A. Zeilinger, Going beyond bell’s theorem, in *Bell’s Theorem, Quantum Theory and Conceptions of the Universe*, edited by M. Kafatos (Springer Netherlands, Dordrecht, 1989) pp. 69–72.
- [86] S. Minsker, Distributed statistical estimation and rates of convergence in normal approximation, *Electronic Journal of Statistics* **13**, 5213 (2019).
- [87] K. Drakakis, A review of the available construction methods for Golomb rulers., *Advances in Mathematics of Communications* **3**, 235 (2009).
- [88] A. J. Ferris and G. Vidal, Perfect sampling with unitary tensor networks, *Physical Review B* **85**, 165146 (2012).
- [89] H.-Y. Huang, R. Kueng, and J. Preskill, Efficient Estimation of Pauli Observables by Derandomization, *Physical*

Appendix A: MoM Bound

We present a proof for the bound

$$P[|\hat{\mu}_N - \mathbb{E}(X)| \geq \varepsilon] \leq 2e^{-k/2}, \quad (\text{A1})$$

where $\varepsilon = \sqrt{4e^2\sigma^2k/N}$ and N is the total number of data points for an MoM estimator $\hat{\mu}_N$, adapted from Devroye et al. [76].

Given random variables X_1, \dots, X_N , we split them into k disjoint sets of size $b = \lfloor N/k \rfloor$, and find their mean. If $|\hat{\mu}_N - \mathbb{E}(X)| \geq \varepsilon$, this means more than half of the means $\bar{X}_i^{(b)} = b^{-1} \sum_{j \in J_i} X_j$, $|J_i| = b$ deviates from $\mathbb{E}(X)$ by more than ε . Let $Y_i^{(b)} = \bar{X}_i^{(b)} - \mathbb{E}(X)$:

$$\sum_{i=1}^k I \{ |Y_i^{(b)}| \geq \varepsilon \} \geq \frac{k}{2}. \quad (\text{A2})$$

As $Y_i^{(b)}$ are i.i.d., let $\text{Var}[X_i] = \sigma^2 < \infty$ and $\text{Var}[Y_i^{(b)}] = k\sigma^2/N$ so that by Chebyshev's inequality,

$$P(|Y_i^{(b)}| \geq \varepsilon) \leq \frac{k\sigma^2}{N\varepsilon^2}. \quad (\text{A3})$$

$|Y^{(l)}| \geq \varepsilon$ is a Bernoulli event with probability $\leq k\sigma^2/N\varepsilon^2$. This implies

$$P\left(\sum_{i=1}^k I \{ |Y_i^{(b)}| \geq \varepsilon \} = r\right) \leq \binom{k}{r} \left(\frac{k\sigma^2}{N\varepsilon^2}\right)^r \left(1 - \frac{k\sigma^2}{N\varepsilon^2}\right)^{k-r}. \quad (\text{A4})$$

Putting everything together,

$$P(|\hat{\mu}_N - \mathbb{E}(X)| \geq \varepsilon) \leq P\left(\sum_{i=1}^k I \{ |Y_i^{(b)}| \geq \varepsilon \} \geq \frac{k}{2}\right) \quad (\text{A5})$$

$$\leq \sum_{r=\lceil k/2 \rceil}^k \binom{k}{r} \left(\frac{k\sigma^2}{N\varepsilon^2}\right)^r \left(1 - \frac{k\sigma^2}{N\varepsilon^2}\right)^{k-r} \quad (\text{A6})$$

$$\leq \left(\frac{k\sigma^2}{N\varepsilon^2}\right)^{\lceil k/2 \rceil} \sum_{r=\lceil k/2 \rceil}^k \binom{k}{r} \quad (\text{A7})$$

$$\leq \left(\frac{k\sigma^2}{N\varepsilon^2}\right)^{\lceil k/2 \rceil} \sum_{r=0}^k \binom{k}{r} \quad (\text{A8})$$

$$= \left(\frac{k\sigma^2}{N\varepsilon^2}\right)^{\lceil k/2 \rceil} 2^k. \quad (\text{A9})$$

Choosing $N = 4e^2\sigma^2k/\varepsilon^2$ ensures that

$$P(|\hat{\mu}_N - \mathbb{E}(X)| \geq \varepsilon) \leq e^{-k} \quad (\text{A10})$$

$$\leq 2e^{-k/2}, \quad (\text{A11})$$

thereby obtaining the bound given in [Equation A1](#).

Appendix B: Bounds for Gaussian Distribution

In the simulations, the mean performed better despite having worse bounds than the MoM estimators when using Chebyshev's inequality ([Equation 8](#)). However, for large shadow size, the distribution of the estimator $\hat{o}_i(N, 1)$

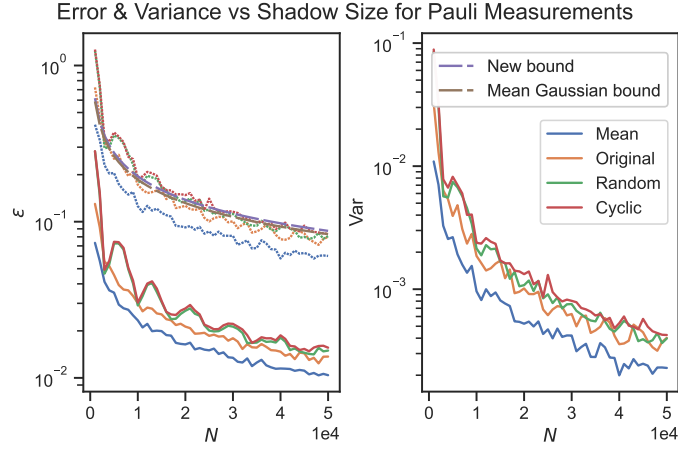


FIG. 9: Error and variance vs shadow size for the Ising model using Pauli measurements when estimating the correlator, as in Figure 2. We compare the bounds under the assumption that the distribution of the mean of the shadow is Gaussian, and the bound by Minsker in Theorem 2.

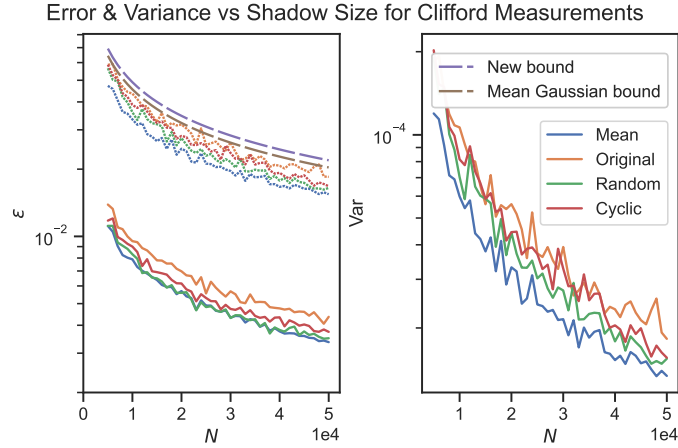


FIG. 10: Error and variance vs shadow size for the 2-qubit GHZ state using Clifford measurements when estimating fidelity, as in Figure 4, with comparison of bounds under the normality assumption.

tends towards a Gaussian distribution, with $P(|\hat{\mu} - \mu| \geq \varepsilon) \leq \exp\left(-\frac{N\varepsilon^2}{2\sigma^2}\right) \equiv \frac{\delta}{M}$, giving an explanation for the better-than-expected performance of the mean. Here, we include comparisons between this tighter bound under this normality assumption, and the bound in Theorem 2.

This ‘Mean Gaussian bound’ is tighter than Theorem 2 and obeyed by the mean for the Ising model (Figure 9), 2-qubit GHZ (Figure 10), 5, 10, 15, 20-qubit GHZ (Figure 11), and GHZ purity (Figure 12). In Figure 11, the tighter bound is obeyed by the mean and MOMRAND, but not MOM and MOMCYC. These results demonstrate the validity of the normality assumption for classical shadows.

Appendix C: Performance of Estimators for Pauli Observables

The performance of the estimators may be explained by the different values of k used for each, as suggested by analysis by Huang et al. [89]. The mean is equivalent to MOM with $k = 1$. For MOM, $k = 43$. For MOMRAND and MOMCYC, $k = [65, 219]$ when $N = [1000, 50000]$. k changes the number of data points $\text{tr}(O_i \hat{\rho}_j)$ that the final estimate is averaged over, corresponding to $\lfloor N/k \rfloor$.

Figure 13 shows that, rather than the type of estimator used, the error depends most heavily on the number of groups k . The fewer data points per group and the higher k used, the higher the error and variance of the estimator.

In the aforementioned paper, Huang et al. showed that the failure probability of the estimator for Pauli observables

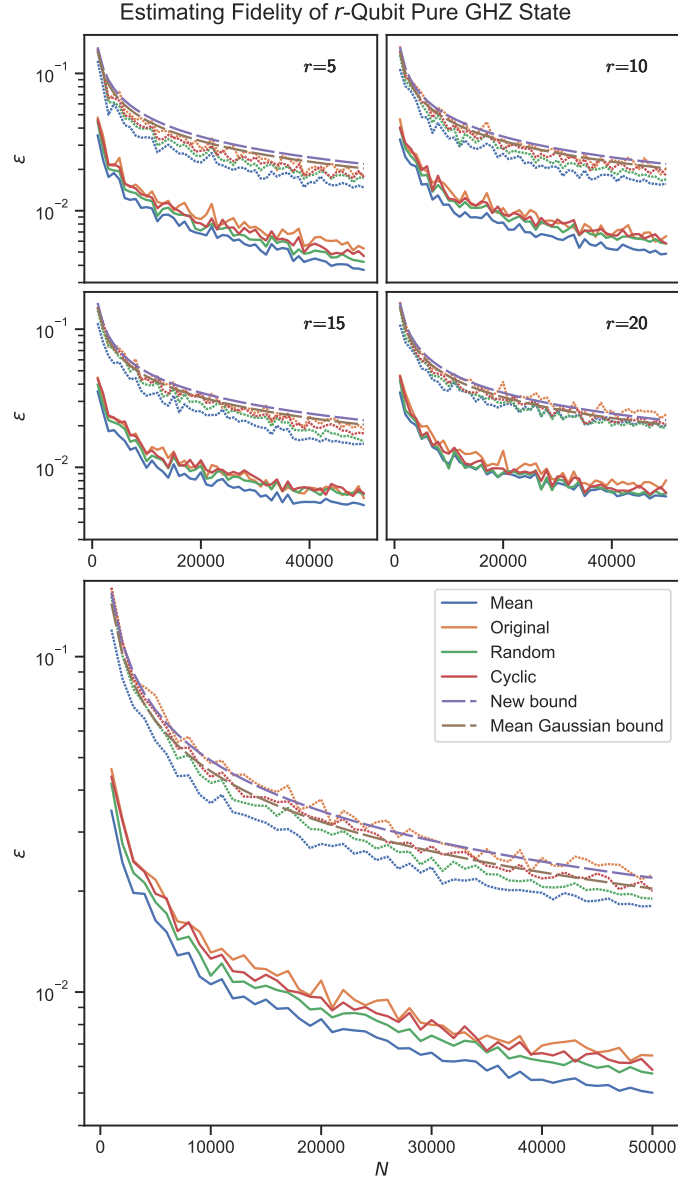


FIG. 11: Error and variance vs shadow size for the 5, 10, 15, 20-qubit GHZ states using Clifford measurements when estimating fidelity, as in Figure 5, with comparison of bounds under the normality assumption.

and measurements is exponentially suppressed by the ‘hit count’ of the estimator. For a system of n_q qubits, we perform N Pauli measurements $p_i \in \{X, Y, Z\}^{n_q}$, to estimate M observables O_j , with each measurement corresponding to a snapshot $\hat{\rho}_i$. For Pauli observables, Equation 37 implies that $\text{tr}(\hat{\rho}_i O_j)$ is non-zero if the measurement ‘hits’ the observable, $O_j \triangleright p_i$. That is, by substituting $\{X, Y, Z\}$ in p_i with I , we can obtain O_j if $O_j \triangleright p_i$. Huang et al. showed that the performance of the estimator improves exponentially with the number of hits. By splitting the data set into groups, the hit count in each group is reduced, exponentially increasing the failure probability of each \bar{X}_i for MOM and \bar{Z}_j for MOMRAND and MOMCYC.

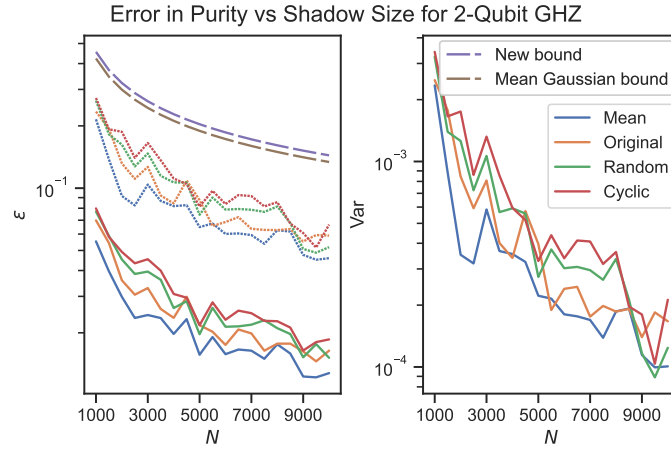


FIG. 12: Error and variance vs shadow size for the 2-qubit GHZ state using Clifford measurements when estimating the purity, as in Figure 8, with comparison of bounds under the normality assumption.

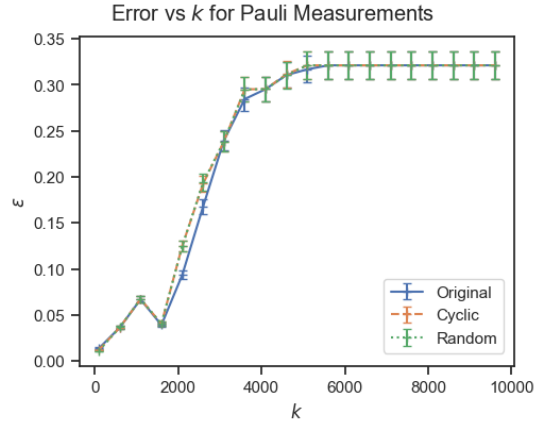


FIG. 13: Error vs group size k for predicting the 2-point correlator for 50 qubits, using different estimators, averaged over 10 independent runs.